

A Review of Experimental and Modeling Techniques to Determine Properties of Biopolymer-Based Nanocomposites

P. Kumar, K.P. Sandeep, S. Alavi, and V.D. Truong

Abstract: The nonbiodegradable and nonrenewable nature of plastic packaging has led to a renewed interest in packaging materials based on bio-nanocomposites (biopolymer matrix reinforced with nanoparticles such as layered silicates). One of the reasons for unique properties of bio-nanocomposites is the difference in physics at nanoscale as compared to that at macroscale. Therefore, the effect of nanoscale on the properties of bio-nanocomposites is discussed. Properties of bio-nanocomposites are governed by the extent of dispersion of nanoparticles in the biopolymer matrix and interaction between nanoparticles and the biopolymer. Selection of proper technique to determine properties of these bio-nanocomposites is very critical in assessing their performance. Experimental techniques (tensile testing, barrier property measurement, dynamic mechanical analysis, differential scanning calorimetry, thermogravimetric analysis, rheological measurement) to determine the mechanical, barrier, thermal, and rheological properties of bio-nanocomposites are discussed in terms of methodology, interpretation of results, and application in studying the properties of bio-nanocomposites. Mathematical modeling plays an important role in predicting the properties of bio-nanocomposites and comparing them to the measured properties. This comparison helps in better understanding the mechanism for much improved properties of bio-nanocomposites. Mathematical modeling is also helpful in understanding the effects of different parameters on the properties of bio-nanocomposites. Therefore, the article describes mathematical modeling of mechanical and barrier properties of bio-nanocomposites using analytical micromechanics.

Keywords: bio-nanocomposites, characterization of properties, experimental techniques, mathematical modeling

Introduction

The nonbiodegradable and nonrenewable nature of plastic packaging has led to a renewed interest in packaging materials based on biopolymers derived from renewable sources. Such biopolymers include naturally occurring proteins, cellulose, starches, and other polysaccharides and those synthesized chemically from naturally derived monomers such as lactic acid. However, biopolymers cannot meet the requirements of a cost-effective film with mechanical and barrier properties matching those of plastics. Recently, a new class of materials represented by bio-nanocomposites has proven to be a promising option in improving the mechanical, barrier, and thermal properties of these biopolymer-based packaging materials. Bio-nanocomposites consist of a biopolymer matrix reinforced with particles (nanoparticles) having at least one dimension in the nanometer range (1 to 100 nm). Bio-nanocomposites exhibit much improved properties as compared to biopolymers

due to the high aspect ratio and high surface area (A_s) of nanoparticles.

Several review articles discuss the preparation, characterization, properties, and applications of bio-nanocomposites (Pandey and others 2005; Ray and Bousmina 2005; Rhim and Ng 2007; Sorrentino and others 2007; Yang and others 2007; Hubbe and others 2008; Zhao and others 2008; Bordes and others 2009; Chivrac and others 2009; Arora and Padua 2010) in food packaging. However, there is a lack of comprehensive review on various analytical and modeling techniques to determine properties of bio-nanocomposites. Properties of interest for application of bio-nanocomposites in food packaging are mechanical, barrier, thermal, and rheological properties. Mechanical properties of interest are tensile modulus (TM), tensile strength (TS), and percent elongation (%E) at break. TM is a measure of the resistance of a material to deformation. TS is the maximum tensile stress a film can sustain, whereas %E is an indication of flexibility of a bio-nanocomposite film. Barrier properties of a packaging material play an important role in determining the shelf life of a food product. Barrier properties of a material indicate their resistance to sorption and diffusion of moisture and gases across the packaging material. Bio-nanocomposite films show improved barrier properties because nanoparticles dispersed in the biopolymer matrix provide a tortuous path for water and gas molecules to pass through. This increases the effective path length for diffusion, thereby improving the barrier properties (Rhim and Ng 2007). Barrier properties of interest in food packaging are water vapor permeability (WVP) and oxygen permeability (OP).

MS 20091112 Submitted 11/6/2009, Accepted 10/5/2010. Authors Kumar and Sandeep are with Dept. of Food, Bioprocessing, and Nutrition Sciences, North Carolina State Univ., Raleigh, NC, U.S.A. Author Alavi is with Dept. of Grain Science and Industry, Kansas State Univ., Manhattan, KS, U.S.A. Author Truong is with U.S. Dept. of Agriculture, Agricultural Research Service, South Atlantic Area, Food Science Research Unit, Raleigh, NC, U.S.A. Direct inquiries to author Sandeep (E-mail: kp_sandeep@ncsu.edu).

Paper nr FSR-09-36 of the Journal Series of the Dept. of Food, Bioprocessing, and Nutrition Sciences, North Carolina State Univ., Raleigh, NC 27695-7624, U.S.A.

Thermal properties of interest for bio-nanocomposites are glass transition temperature (T_g), thermal stability, and heat deflection temperature (HDT). Rheological properties of a material are important to understand the processability of the material. Rheological measurements indicate melt-processing behavior of bio-nanocomposites during unit operations such as injection molding and blown film process. These properties of bio-nanocomposites are governed by the extent of dispersion of nanoparticles in the biopolymer matrix and interaction between nanoparticles and the biopolymer. Selection of proper technique to determine properties of these bio-nanocomposites is very critical in assessing their performance.

Mathematical modeling plays an important role in predicting the properties of bio-nanocomposites and comparing them to the measured properties. Mathematical modeling methods to predict properties of nanocomposites include the techniques of computational chemistry and computational mechanics. Computational chemistry makes use of modeling tools such as quantum mechanics and nanomechanics. Nanomechanics assumes a noncontinuous composition of material and studies atomic interactions at the nanoscale. Nanomechanics includes techniques such as molecular dynamics, Monte Carlo, and *ab initio* simulations. Molecular dynamics predicts interaction between constituent phases of a composite at the atomic scale. Monte Carlo simulation is a probabilistic model for the prediction of properties of a system. *Ab initio* simulation, based on 1st principles, involves the solution of Schrodinger's wave equation for each electron (Valavala and Odegard 2005). Nanomechanics techniques can predict properties of a wide range of nanocomposite systems. However, these techniques are computationally very exhaustive. Further details on these nanomechanics techniques can be found in a review article by Valavala and Odegard (2005).

The computational mechanics makes use of modeling tools such as micromechanics and structural mechanics. Micromechanics assumes the presence of a continuous structure of materials and does not include any chemical interactions. Micromechanics includes techniques such as computational micromechanics (finite element method, boundary element method) and analytical micromechanics (Rule of mixtures, Halpin-Tsai method, Mori-Tanaka theory) (Valavala and Odegard 2005). Most of this review focuses on mathematical modeling using analytical micromechanics, which has been widely used to model the properties of nanocomposites (Fornes and Paul 2003; Luo and Daniel 2003; Sheng and others 2004; Wu and others 2004; Weon and Sue 2005; Yung and others 2006; Rao 2007). The same modeling concepts can be applied for modeling the properties of bio-nanocomposites.

This article presents a review of experimental and modeling techniques to determine properties of bio-nanocomposites. Effect of nanoscale on the properties of bio-nanocomposites is discussed. Experimental techniques to determine the mechanical, barrier, thermal, and rheological properties of bio-nanocomposites are also discussed. Lastly, the article describes mathematical modeling of mechanical and barrier properties of bio-nanocomposites using analytical micromechanics.

Effect of Nanoscale on Properties

Physics at nanoscale

One of the reasons for unique properties of materials at nanoscale is the difference in physics at nanoscale as compared to that at macroscale. The fundamental laws of physics remain same. However, their relative importance changes at the nanoscale.

Gravitational and inertial forces are volume forces (force is directly proportional to volume). Volume forces are dominant only at the macroscale and they become almost negligible at the nanoscale. Frictional force is a volume force at macroscale. However, frictional force becomes surface force (force is directly proportional to A_s) at nanoscale because adhesive forces between atoms and molecules become considerable at nanoscale (Rogers and others 2008). It has also been reported that water exhibits much higher viscosity at nanoscale as compared to that of bulk water (Li and others 2007).

Electrostatic and van der Waals forces are 2 major forces that become dominant at nanoscale. Electrostatic forces, which can be either repulsive or attractive, are very strong and act at a length scale of 1 to 100 nm. van der Waals forces are attractive and act at distances less than 2 nm. There are 3 types of van der Waals forces: (i) dipole-dipole force (orientation or Keesom force) occurs between polar molecules such as water, (ii) dipole-induced dipole force (induction of Debye force) arises when a polar molecule polarizes a nearby nonpolar molecule, and (iii) induced dipole-induced dipole force (dispersion of London force) acts on all atoms and molecules and is the most important van der Waals force (Eijkel and van den Berg 2005; Rogers and others 2008).

Another difference between macroscale and nanoscale is the quantum mechanics. Quantum mechanics, instead of classical mechanics, describes the motion and energy at the nanoscale. Quantum mechanics considers the wave-particle duality of electrons. A material can exhibit totally new properties with only a reduction in size because of the wave-particle duality of electrons. For example, gold at macroscale is yellow, inert, and nonmagnetic metal at macroscale. However, 10 nm particles of gold appear red, exhibit catalytic activity, and are magnetic (Roduner 2006).

Another distinctive effect that becomes dominant at the nanoscale is the Brownian motion. Nanoscale materials undergo a random type of motion, known as the Brownian motion. Brownian motion arises because atoms are in a state of constant motion (Jones 2004).

Higher A_s to volume (V_s) ratio

A_s to V_s ratio is an indication of the quantity of interfacial region as compared to the bulk region in a composite. The interfacial region controls formation of new structural arrangements on the molecular scale. The A_s to V_s ratio for a spherical particle with radius r is given as (Crosby and Lee 2007):

$$\frac{A_s}{V_s} = \frac{4\pi r^2}{\frac{4}{3}\pi r^3} = \frac{3}{r} \quad (1)$$

Nanoparticles have higher A_s to V_s ratio because of their very small size (1 to 100 nm). Higher A_s to V_s ratio results in greater interfacial region, resulting in increased interaction between the polymer chain and the nanoparticles. This increased interaction improves the properties of the bio-nanocomposites. Other than size, shape is an important factor in determining A_s to V_s ratio (Crosby and Lee 2007). The high A_s to V_s ratio also makes nanoparticles more reactive as catalysts in chemical reactions.

Confinement effect

For nanoscale particles, a very small volume fraction is sufficient to achieve average distances between particles of the same order of magnitude as the radius of gyration of the macromolecules. Thus, the polymer molecule can be confined between 2 nanoscale

particles. This is known as the confinement effect. Confinement effect reduces the number of conformations of the polymer molecules. Confinement effect is also responsible for reducing gas permeability value by providing tortuous paths for a gas molecule to diffuse through the nanocomposite (Damme 2008).

Experimental Techniques to Determine Properties

Mechanical properties

Tensile testing. Tensile testing is done to measure the mechanical properties of materials. Tensile testing of a bio-nanocomposite film can be done according to ASTM D882-02 or ASTM D638-03. ASTM D638-03 can be used to test materials of thickness up to 14 mm. ASTM D882-02 is the preferred method to do tensile testing of materials in the form of thin sheets of less than 1 mm in thickness. During tensile testing, a rectangular specimen is placed in the grips of movable and stationary fixtures in a testing machine capable of moving the movable fixture at a constant velocity away from the stationary fixture. One such testing machine commonly used for tensile testing of bio-nanocomposite films is Universal Testing Machine. The sample is pulled apart until it breaks. The applied load (force) and the resulting elongation of the specimen are measured (ASTM Standards 2002, 2003).

Mechanical properties of a sample are determined from the force-elongation curve (Figure 1). TM is the slope of the initial linear portion of stress-strain curve. TM, also known as the Young's modulus or the modulus of elasticity, is calculated as:

$$TM = \frac{\frac{\Delta F}{A_i}}{\frac{\Delta L}{L_i}} \quad (2)$$

where ΔF and ΔL are the corresponding changes in force and length during the initial linear deformation. A_i is the initial minimum cross-sectional area of the specimen and L_i is the initial gauge length of the specimen in between the grips of the instrument.

TS is a measure of the strength of a material under tensile loading and is calculated as:

$$TS = \frac{F_B}{A_i} \quad (3)$$

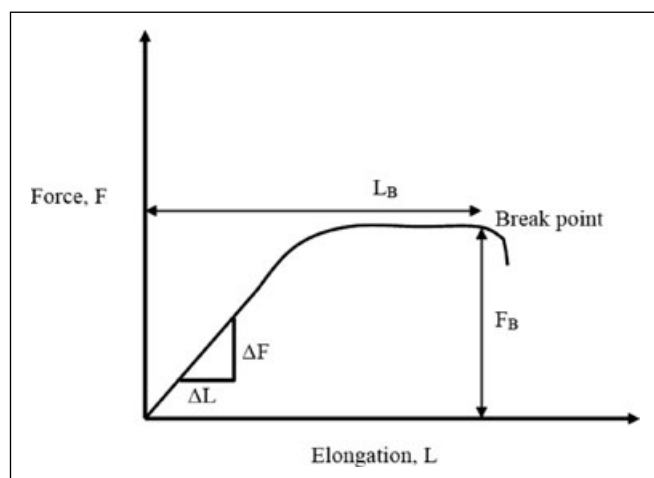


Figure 1—A typical force-elongation curve during a tensile testing experiment.

where F_B is the force at break point. %E at break is the extent to which a material can be stretched before it breaks. It is calculated as:

$$\%E = \frac{L_B}{L_i} \times 100 \quad (4)$$

where L_B is the elongation at break point. Toughness (tensile energy to break) of a sample is the energy required to break the sample and is calculated from the area under the force-elongation curve. It is a measure of the energy a sample can absorb before it breaks (ASTM Standards 2002; Bhattacharya and others 2007).

Most studies on tensile testing of bio-nanocomposites report TS and %E as a function of the nanoparticle content. Chen and Zhang (2006) reported an increase in TS of soy protein-montmorillonite (MMT) nanocomposite sheets from 8.77 to 15.43 MPa as the MMT content was increased to 16%. %E at break of bio-nanocomposite sheets decreased with increasing MMT content. Yu and others (2007) reported similar results for soy protein-rectorite nanocomposite sheets. The TS reached a maximum of 12.92 MPa at rectorite content of 12%. %E at break of soy protein-rectorite nanocomposite sheets decreased with increasing rectorite content. Similar results on the tensile testing of bio-nanocomposites based on other biopolymers have been reported (Chang and others 2003; Park and others 2004; Jeong and others 2005; Wang and others 2005; Huang and Netravali 2006; Rao 2007; Zheng and others 2007; Chivrac and others 2008; De Moura and others 2008; Rimdusit and others 2008; Roohani and others 2008; Tang and others 2008; Chang and others 2009; Azeredo and others 2010).

Dogan and McHugh (2007) investigated the effect of size of microcrystalline cellulose (MCC) on composite films based on hydroxyl propyl methyl cellulose (HPMC) and MCC. The TS of the composite films increased from 29.7 to 70.1 MPa with the addition of 500 nm size particles. However, TS increased only to 37.4 with the addition of 3- μ m size particles. This was attributed to the increased A_s of the particles with smaller size, increasing the hydrogen bonding of MCC with the HPMC matrix.

Barrier properties

Water vapor permeability. WVP is the rate of water vapor transmission through unit area of a flat material of unit thickness induced by unit vapor pressure difference across the material. WVP of a bio-nanocomposite film can be determined according to ASTM E96-05. There are 2 basic methods: desiccant method and water method. In the desiccant method, test specimen is sealed to the top of a test dish containing a desiccant such as calcium chloride. The desiccant maintains 0% relative humidity inside the test dish. The test assembly is placed in an atmosphere of known relative humidity and temperature. Periodic weighing of the test dish determines the rate of water vapor transmitted through the specimen into the dish. In the water method, test dish contains distilled water that maintains a relative humidity of 100% inside the dish. Periodic weighing determines the amount of water vapor lost from the test dish to the controlled atmosphere (ASTM Standards 2005a). Water vapor transmission rate (WVTR) is calculated as (ASTM standards 2005a):

$$WVTR = \frac{Q}{t A} \quad (5)$$

where Q is the change in weight, t is the time, and A is the area of the mouth of the cup. WVP is calculated as (ASTM standards 2005a):

$$WVP = \frac{WVTR \times \Delta x}{\Delta p} \quad (6)$$

where Δx is the thickness of the test specimen and Δp is the vapor pressure difference across the test specimen.

Tang and others (2008) reported WVP of starch-clay bio-nanocomposite films with 3 different kinds of starches (corn, wheat, and potato starch) and 2 different types of clay (natural MMT and modified MMT). The bio-nanocomposite films were prepared by melt extrusion followed by film casting. At the same clay content, WVP of starch-natural MMT films was significantly lower than that of starch-modified MMT films. The results showed that WVP of bio-nanocomposite films decreased significantly with an increase in natural MMT content. WVP of wheat starch film with MMT content of 21% was 70% lower than that of wheat starch film with no MMT (Tang and others 2008). Similar results on the WVP of bio-nanocomposite films based on other biopolymers have been reported (Park and others 2004; Rhim and others 2006; Dogan and McHugh 2007; Tunc and others 2007; Rhim and others 2009; Azeredo and others 2010).

De Moura and others (2008) reported WVP of bio-nanocomposites based on HPMC and chitosan nanoparticles. The value of WVP decreased significantly with the addition of chitosan nanoparticles. However, no significant changes in WVP values were observed with varying concentrations for nanoparticles of sizes 59 and 82 nm. WVP value for films containing 100 nm nanoparticles decreased significantly with an increase in nanoparticles content.

Oxygen permeability. OP is the rate of oxygen transmission through unit area of a flat material of unit thickness induced by unit vapor pressure difference across the material. OP of a bio-nanocomposite film can be determined according to ASTM E3985-05. The specimen is mounted between 2 chambers under ambient conditions. One chamber is slowly purged by a stream of nitrogen, while the other chamber contains oxygen. Oxygen from the other chamber permeates through the test specimen into the chamber with nitrogen. Oxygen is transported by the carrier nitrogen gas to the coulometric detector, where it produces an electrical current. The magnitude of electric current is proportional to the amount of oxygen flowing into the detector per unit time (ASTM standards 2005b).

Oxygen transmission rate (OTR) is calculated as (ASTM standards 2005b):

$$OTR = \frac{(V_e - V_0) \times Q_c}{A R_L} \quad (7)$$

where V_e is the steady state voltage level, V_0 is zero voltage level, Q_c is the calibration constant, A is the exposed area of the test specimen, and R_L is the value of load resistance.

OP is calculated as (ASTM standards 2005b):

$$OP = \frac{OTR \times \Delta x}{p} \quad (8)$$

where Δx is the thickness of the test specimen and p is the partial pressure of oxygen in the oxygen chamber.

Ray and others (2003a) determined OP of bio-nanocomposites based on polylactide and modified MMT. The results showed a

19% decrease in OP as the MMT content increased to 7%. Chang and others (2003) reported OP values of bio-nanocomposites based on polylactic acid (PLA) and clay nanoparticles. The value of OP decreased from 777 to 327 cc/m²/d as the clay content increased from 0% to 10%. De Moura and others (2008) reported OP of bio-nanocomposites based on HPMC and chitosan nanoparticles. The value of OP decreased significantly as the particle size of the chitosan nanoparticles decreased from 110 to 59 nm. The value of OP also decreased significantly as the content of chitosan nanoparticles increased.

Thermal properties

The techniques for characterization of thermal properties of bio-nanocomposites include dynamic mechanical analysis (DMA), differential scanning calorimetry (DSC), and thermogravimetric analysis (TGA).

Glass transition temperature. Thermal transitions such as glass transition in a polymer can be described by either free volume (volume available to a molecule for internal movement) theory or relaxation time. As the temperature increases, free volume increases. This enables movements of bonds (bending and stretching) and side chains. This transition, corresponding to bending and stretching of bonds, is known as the γ -transition. β -transition is associated with the movement of side chains and is related to the toughness of the material. With further increase in temperature, free volume further increases and there is a large-scale movement of polymer chains. This thermal transition is known as the α -transition or glass transition and the associated temperature is known as the T_g . T_g is the temperature at which an amorphous solid changes from a relatively brittle (glassy) to a softer (rubbery) material. At the T_g , there is an abrupt change in properties such as storage modulus, specific heat, and coefficient of expansion (Menard 1999).

DMA and DSC are the 2 main techniques used to determine the T_g . DMA is a sensitive technique that can be used to detect β - and γ -transitions that cannot be detected by methods such as DSC (Menard 1999).

Dynamic mechanical analysis. DMA or dynamic mechanical thermal analysis (DMTA) is a method to characterize viscoelastic behavior of a material. This is done by measuring the response of a material to an oscillating force as a function of temperature. The oscillating force applies a sinusoidal stress ($\sigma = \sigma_0 \sin \omega t$) to the sample. This generates a sinusoidal strain. The amplitudes of deformation at the peak of sine wave and lag between stress and strain sine waves are measured. From these measurements, a complex modulus ($E^* = E' + iE''$) is calculated. Storage modulus (E') is defined as the stress in phase with the strain divided by the strain under a sinusoidal deformation. It is a measure of the ability of a material to store energy. Loss modulus (E'') is defined as the stress out of phase with the strain divided by strain. It is a measure of the ability of a material to dissipate energy. Ratio of storage modulus and loss modulus is known as the loss tangent ($\tan \delta = E''/E'$). Complex modulus can be used to calculate complex shear modulus (G^*) and complex viscosity (η^*) of a material as (Menard 1999):

$$G^* = \frac{E^*}{2(1 + \nu)}$$

$$\eta^* = \frac{G^*}{\omega} \quad (9)$$

where ν is Poisson's ratio and ω is the frequency of oscillation.

DMA should be conducted in the linear viscoelastic region because the viscoelastic behavior of a material is independent of deformation in this region. This region can be determined by either creep recovery or dynamic strain sweep test. Creep recovery test applies a constant stress to a material and monitors resulting strain with time. Linear viscoelastic region is determined by running a series of creep recovery tests on a material at different stress values and plotting creep compliance as a function of time. Compliance is the ability of a material to deform and is the inverse of the complex modulus. The compliance curves should overlap in the linear viscoelastic region (Menard 1999). Dynamic strain sweep test applies increasing stress and strain at a constant frequency. The range of strain or stress in which complex modulus or complex viscosity remains constant is the linear viscoelastic region for the material at the given frequency (Bhattacharya and others 2007).

T_g can be determined by performing a DMA experiment as the temperature is increased at a constant heating rate according to ASTM E1640-04 (ASTM standards 2004) and ASTM D4065-06 (ASTM standards 2006). Samples can be tested under different configurations such as tension, compression, 3-point bending, single cantilever, dual cantilever, and torsion. The choice of configuration depends on the type of material, modulus of material, and the type of stress the material is exposed to. Flexible materials such as thin films are often tested under tension mode, whereas stiff materials such as composites are tested under 3-point bending mode (Menard 1999).

A typical temperature scan during a DMA experiment is shown in Figure 2. T_g can be determined from changes in one of the 3 parameters: the peak of $\tan \delta$ curve, peak of E'' curve, or onset point for abrupt decrease in E' value. The parameter used to detect the glass transition should always be reported. The part of the region above glass transition and below melting temperature is known as the rubbery plateau region. The storage modulus in the plateau region is proportional to either the number of cross-links or the chain length between entanglements of polymer chains. The length of the plateau region increases as the molecular weight (M_e) of the entanglement of polymer chains increases. The rubbery plateau is also related to the crystallinity of a material. On further heating, melting point is reached. At the melting point, the polymer chains start sliding past each other and the material flows (Menard 1999).

T_g is significantly affected by testing parameters such as frequency of oscillation and heating rate. The most commonly used frequency for a DMA experiment is 1 Hz. However, frequency for performing a DMA experiment should be chosen properly. Frequency scan determines the response of a material over various shear rates. At very low frequencies, materials exhibit Newtonian behavior. Viscosity in this region is dependent on the molecular weight (M_v) as (Menard 1999):

$$\eta = c(M_v)^a \quad a = 1 \text{ for } M_v < M_e \text{ and } 3.4 \text{ for } M_v > M_e \quad (10)$$

where c is a material constant. As the frequency increases, materials exhibit non-Newtonian behavior. Viscosity in this region can be determined by the power-law model as (Menard 1999):

$$\sigma = K(\dot{\gamma})^n \quad (11)$$

where σ is the shear stress, $\dot{\gamma}$ is the shear rate, K is the consistency coefficient, and n is the flow behavior index. As the frequency increases further, materials exhibit Newtonian behavior once again.

This region is known as the infinite shear plateau region. The material is not able to show a response to increase in shear rate in this region. This region is usually avoided in DMA because there is no entanglement of the polymer chains. Temperature of thermal transition shifts to a higher temperature as the test frequency is increased. Ideally, the frequency should be the one that the material is exposed to during the processing under consideration. Another approach is to scan across the frequency range of interest by holding the temperature constant (Menard 1999). Heating rate of a DMA test should be slow enough to allow the entire specimen to reach equilibrium. The most commonly used heating rate for a DMA experiment ranges from 3 to 5 °C/min. Temperature of thermal transition shifts to a higher temperature as the heating rate is increased (ASTM standards 2004).

Most studies on DMA of bio-nanocomposites report temperature dependence of E' , E'' , and $\tan \delta$ as a function of the nanoparticle content. Shih and others (2007) reported higher E' of bio-nanocomposites based on polybutylenes succinate (PBS) and modified MMTs than that of neat poly(butylenes succinate). The $\tan \delta$ curve became broader and the peak temperature (T_g) increased with the addition of clay nanoparticles. This was attributed to the confinement of molecular motion of PBS molecules due to clay nanoparticles. Rimdusit and others (2008) reported an increase in T_g , corresponding to the peak of $\tan \delta$ curve, for bio-nanocomposites based on methyl cellulose and MMT. This increase was attributed to restricted segmental motion of biopolymer chains in bio-nanocomposites. Similar results on increase in E' and T_g of bio-nanocomposites based on other biopolymers have been reported (Ray and others 2002b; Huang and Netravali 2006; Sasmal and others 2008; Romero and others 2009).

Park and others (2004) reported temperature dependence of E' and T_g for bio-nanocomposites based on cellulose acetate, triethyl citrate (as plasticizer), and organically modified clay. E' and T_g of the bio-nanocomposites decreased as the plasticizer content increased. E' value (2.25 GPa) of bio-nanocomposite at 30 °C with 40% plasticizer was less than half as compared to that (5.71 GPa) with 20% plasticizer content. This was attributed to the increased segmental motion in cellulose acetate backbone with increase in plasticizer content. The broadening and increase of T_g , as determined by the peak of $\tan \delta$ curve, after addition of modified clay was attributed to the restricted segmental motion of cellulose acetate matrix by clay nanoparticles.

Differential scanning calorimetry. DSC can also be used to determine T_g because it can measure the heat capacity of a material. A small quantity (5 to 20 mg) of sample is placed in a container (sample pan) and an inert material of known heat capacity ($C = mc_p$) is placed in another similar container (reference pan). Both pans are placed inside a calorimeter receptor. A heating element is used to heat the sample pan at a constant rate of temperature increase, set to match the temperature of the reference pan. The result is a thermogram that gives the rate of heat input versus temperature. There is a sudden increase in the heat input corresponding to the T_g (ASTM standards 2008a, 2008b). Apart from determining T_g , DSC can also be used to investigate the melting point and degree of crystallization of bio-nanocomposites.

Most studies on DSC of bio-nanocomposites report temperature-dependent heat flow as a function of the nanoparticle content. Rao (2007) reported a slight increase in melting point of bio-nanocomposites based on gelatin and MMT with an increase in MMT content. Hedenqvist and others (2006) reported a 5 to 10 °C increase in T_g of bio-nanocomposite films based on whey protein and MMT with the addition of MMT. Rimdusit

and others (2008) reported T_g of bio-nanocomposites based on methyl cellulose and MMT. T_g values were taken as the midpoint temperature of the change in specific heat in the transition region. T_g value of the bio-nanocomposites increased from 176 to 182 °C with the increase in MMT content. This increase in T_g was attributed to the restricted thermal motion of methyl cellulose polymer due to MMT nanoparticles. A similar increase in T_g , as determined by DSC, of bio-nanocomposites have been reported (Chang and others 2009; Krishnamachari and others 2009; Azeredo and others 2010).

Thermal stability

Thermogravimetric analysis. Thermal stability of polymeric materials is usually studied by TGA according to ASTM E1131-08 (ASTM standards 2008c). TGA involves continuous monitoring of weight of a sample (10 to 20 mg) in a controlled environment of air or nitrogen as a function of temperature and/or time. A heating element provides controlled heating to the sample and an electrobalance continuously measures the weight. During TGA, the weight loss due to the formation of volatile products is plotted against temperature in a thermogram. Weight loss over specific temperature ranges and environments provides a mechanism for compositional analysis of the material. TGA is also used to determine the clay content of a bio-nanocomposite because clay minerals such as MMT are thermally stable up to a temperature of 900 °C.

Chen and Zhang (2006) reported improved thermal stability of bio-nanocomposites based on soy protein isolate and MMT. With an increase in MMT content, weight loss of the bio-nanocomposites was delayed at temperatures higher than 300 °C. The residual weight at 800 °C was also higher for bio-nanocomposites. Similar results on TGA of bio-nanocomposites based on other biopolymers have been reported (Chang and others 2003; Paul and others 2003; Huang and Netravali 2006; Wang and others 2006; Chiou and others 2007; Shih and others 2007; Tunc and others 2007; Rimdusit and others 2008; Krishnamachari and others 2009).

Wang and others (2006) investigated thermal stability of bio-nanocomposites of chitosan and MMT by TGA under nitrogen

and air flow from room temperature to 800 °C. The thermal degradation of bio-nanocomposites under nitrogen flow was different than that under air flow. Under nitrogen flow, a nonoxidative degradation occurs whereas the sample undergoes an oxidative degradation under air flow.

Heat deflection temperature

HDT is the temperature at which a polymer sample deforms under a specified load. It is an indication of heat resistance of a material to an applied load. HDT of a bio-nanocomposite can be determined according to ASTM D648-07.

This test method applies to rigid or semi-rigid materials with a thickness of 3 mm or higher. According to ASTM method, a rectangular cross-section specimen is tested in 3-point bending by applying a load at its center that provides a maximum stress of 0.455 MPa or 1.82 MPa. The temperature is raised at 2 ± 0.2 °C/min. The temperature at which the test specimen deflects by 0.25 mm is recorded as the HDT (ASTM standards 2007).

Ray and others (2003a) reported HDT of bio-nanocomposites based on polylactide and modified MMT. HDT of the bio-nanocomposites increased from 76 to 111 °C as the MMT content increased to 7%. Park and others (2004) reported HDT of bio-nanocomposites based on cellulose acetate, triethyl citrate (as plasticizer), and organically modified clay. At a plasticizer content of 20%, HDT increased from 95 to 107 °C as the clay content increased from 0% to 5%. At a clay content of 5%, HDT decreased from 107 to 60 °C as the plasticizer content increased from 20% to 40%. Shelley and others (2001) estimated HDT from the storage modulus curve of DMA. HDT was defined as the temperature at which the storage modulus drops to 25% of its value at room temperature.

Rheological properties

Steady shear measurement. Steady shear measurements for bio-nanocomposites are carried out using either the rotational or capillary rheometers. Rotational rheometers with parallel plate or cone and plate geometry are suitable for low to medium range shear rate (<10/s) measurement, whereas capillary rheometers are suitable for high shear rate measurement. Measurements at high

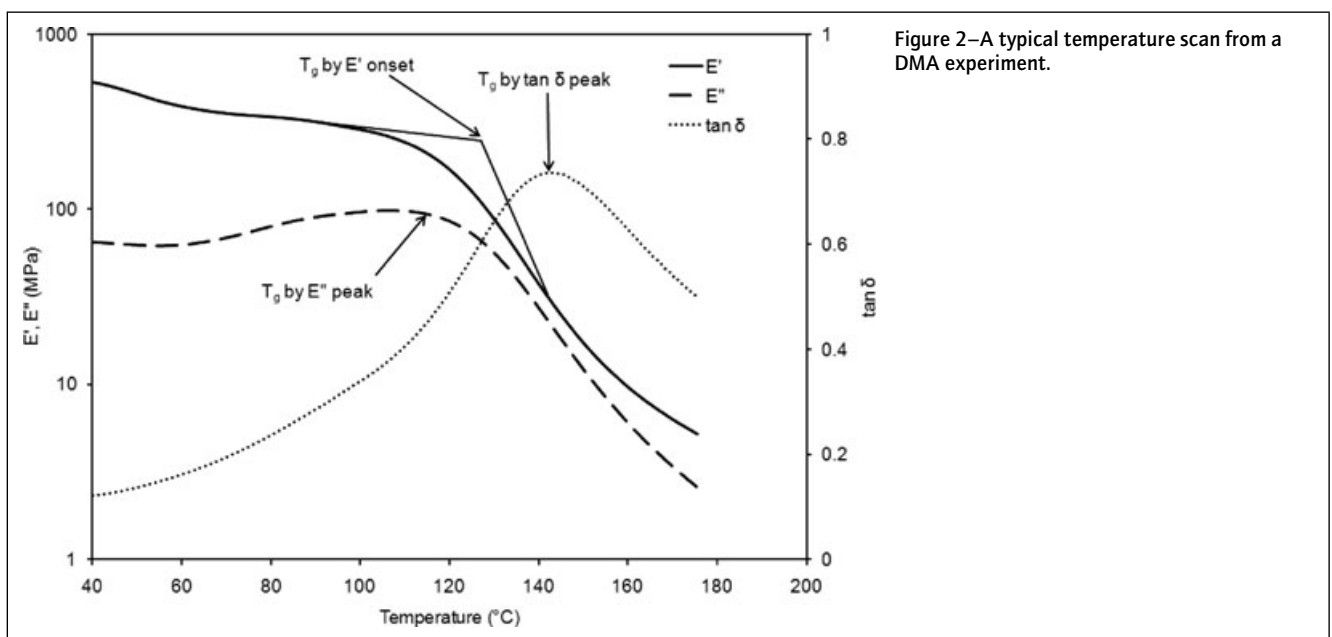


Figure 2—A typical temperature scan from a DMA experiment.

shear rate are necessary to describe flow behavior in processes such as injection molding (Bhattacharya and others 2007).

Dynamic shear measurement. Steady shear measurements can change the microstructure and morphology of bio-nanocomposites. Therefore, dynamic shear measurement is used to study the microstructure of bio-nanocomposites by subjecting them to small deformation. Dynamic shear measurements should be conducted in the linear viscoelastic region because the viscoelastic behavior of a material is independent of deformation in this region. Dynamic shear measurements can be performed by creep recovery, stress relaxation, or dynamic oscillatory deformation (Bhattacharya and others 2007).

In the creep tests, a small stress is applied and the increase in strain is measured, whereas in stress relaxation, a small strain is applied and the decay of stress is measured. During dynamic oscillatory deformation, a small amplitude sinusoidal strain is applied on a sample and the resulting sinusoidal stress is measured. Parameters obtained by dynamic oscillatory deformation include complex shear modulus ($G^* = G' + iG''$) and complex viscosity (η^*) (Bhattacharya and others 2007).

Extensional measurement. Apart from shear, a polymer is also associated with extensional flow in processes such as film blowing, blow molding, and injection molding. Extensional viscosity is a measure of the resistance of a material subjected to stretching. The 2 most common methods for measuring extensional properties are the Meissner-type rheometer and continuous drawing of a monofilament. The main parameter obtained by Meissner-type rheometer is the transient extensional viscosity. Continuous drawing method gives a qualitative measure of the extensional rheology (Bhattacharya and others 2007).

Rheological studies of bio-nanocomposites have focused on steady and dynamic shear measurements as a function of nanoparticle concentration. Apparent viscosity and shear thinning properties of bio-nanocomposites are obtained from steady shear measurements. The steady shear measurements also provide information on the effect of shear on the orientation of nanoparticles in bio-nanocomposites. The dynamic shear measurements on polymer-based nanocomposites have shown a transition from liquid-like to solid-like rheological behavior at relatively low loading of nanoparticles. This has been attributed to the formation of a percolated network of the exfoliated layers of nanoparticles within the nanocomposite matrix (Krishnamoorti and Yurekli 2001).

Ray and others (2003b) reported steady shear and dynamic oscillatory shear measurements for suspensions of bio-nanocomposites based on poly(butylene succinate) and modified MMT. At 120 °C, the steady shear measurements showed that the neat poly(butylene succinate) exhibited Newtonian behavior, whereas bio-nanocomposites exhibited non-Newtonian behavior. High viscosity of bio-nanocomposites at low shear rates was explained by the flow restriction of biopolymer chains in molten state due to the presence of nanoparticles. At very high shear rate, the viscosities of the bio-nanocomposites were comparable to that of neat poly(butylene succinate). This was attributed to strong orientation of clay layers along the direction of flow. A similar result was reported for dynamic oscillatory measurements of these bio-nanocomposites. Similar results on shear thinning behavior of bio-nanocomposites based on other biopolymers have also been reported (Tunc and others 2007).

Chiou and others (2005) studied dynamic rheological behavior of starch-clay suspensions containing different types of starches and MMTs. Samples of natural MMT had the highest G' . There was a 2 order of magnitude increase in G' with an increase in

natural MMT content from 2.5% to 10%. The corresponding increase for other modified MMTs was only one order. This was attributed to the hydrophilic nature of natural MMT as compared to the modified MMTs used in the study. As compared to samples of modified MMTs, samples of natural MMT also had a larger value of G' at temperatures as high as 95 °C. Chivrac and others (2008) reported increased melt viscosity of intercalated bio-nanocomposites based on starch and MMT. This was attributed to the inability of large stacks of MMT layers to orient by shear stress. On the contrary, well-exfoliated bio-nanocomposites based on starch and modified MMT did not show increase in melt viscosity.

Mathematical Modeling of Properties

Modeling of Mechanical Properties

One of the earliest theories for the determination of modulus of a composite system is based on Einstein's equation for the viscosity of a suspension of rigid spheres at very low concentration and is given as (Ahmed and Jones 1990):

$$E_c = E_m(1 + K_E \phi_f) \quad (12)$$

where E_c is the tensile or elastic modulus of the composite, E_m is the tensile or elastic modulus of the matrix, K_E is Einstein's coefficient, and ϕ_f is the volume fraction of the filler. Value of K_E for spherical filler particles is 2.5. Guth generalized Einstein's equation to account for interaction between fillers and obtained the following equation for spherical fillers (Ahmed and Jones 1990):

$$E_c = E_m[1 + K_E \phi_f + 14.1(\phi_f)^2] \quad (13)$$

Guth also developed the following equation for nonspherical fillers (Ahmed and Jones 1990):

$$E_c = E_m[1 + 0.67 \alpha \phi_f + 1.62(\alpha \phi_f)^2] \quad (14)$$

where α is the shape factor or the aspect ratio and is given as the ratio of length to thickness of the filler. However, these equations were only valid for low filler concentration. Mooney further modified Einstein's equation for spherical fillers at higher concentration. Mooney's equation for determining the elastic modulus of a composite system can be generalized as (Rao 2007):

$$\ln \frac{E_c}{E_m} = \frac{K_E \phi_f}{1 - \frac{\phi_f}{\phi_m}} \quad (15)$$

where ϕ_m is the maximum packaging efficiency of the filler that is the ratio of the true volume of the filler to the apparent volume occupied by the filler. Value of ϕ_m for close packed spheres is 0.74. The value of K_E depends on the interaction between filler and the matrix and is related to the aspect ratio ($\alpha = L/t$) through the following equation (Rao 2007):

$$K_E = 2.5 \left(\frac{L}{t} \right)^{0.645} \quad (16)$$

where L and t are the length and thickness of the filler particles, respectively.

Elastic modulus of a composite can also be predicted by the rule of mixtures (Fornes and Paul 2003):

$$E_c = (1 - \phi_f)E_m + \phi_f E_f \quad (17)$$

where E_f is the elastic modulus of the filler. Cox modified the rule of mixtures by introducing a length-dependent efficiency factor (η_l) as (Tucker and Liang 1999):

$$E_c = (1 - \phi_f)E_m + \eta_l \phi_f E_f \quad (18)$$

where

$$\eta_l = \left[1 - \frac{\tanh\left(\frac{\beta L}{2}\right)}{\left(\frac{\beta L}{2}\right)} \right] \quad (19)$$

and

$$\beta^2 = \frac{H}{\pi r_f^2 E_f}, \quad H = \frac{2\pi G_m}{\ln\left(\frac{R}{r_f}\right)} \quad (20)$$

where r_f is the radius of the filler, R is the radius of the matrix, and G_m is the shear modulus of the matrix. R can be calculated as (Tucker and Liang 1999):

$$\frac{R}{r_f} = \sqrt{\frac{K_R}{\phi_f}} \quad (21)$$

where the value of K_R is 3.628. Verbeek (2003) further modified Cox's model by assuming perfect adhesion between individual components of the composite. Transfer of stress was explained by a shear mechanism. Similar to efficiency factor (η_l), a modulus reduction factor (MRF) was introduced in the equation for modulus as (Verbeek 2003):

$$E_c = (1 - \phi_f)E_m + (MRF)\phi_f E_f \quad (22)$$

where

$$MRF = \left[1 - \frac{\tanh(\kappa)}{(\kappa)} \right] \quad (23)$$

and

$$\begin{aligned} \kappa &= \alpha \sqrt{\frac{(1 - \chi)^3 G_m}{E_f} \left(\frac{\phi_f}{1 - \phi_f} \right)} \\ \chi &= \frac{\phi}{(1 - \phi_f)(1 - \phi) + \phi} \\ \phi &= \frac{\phi_f^2 \phi_m}{1 - (1 - \phi_f)\phi_m} \end{aligned} \quad (24)$$

where ϕ is the porosity of the composite and χ is the modified porosity (porosity relative to polymer phase).

Nielsen (1977) proposed a power law equation to predict properties of composites with one continuous phase and one dispersed phase. The power law equation can be given as (Nielsen 1977):

$$E_c = (1 - \phi_f)E_m^n + \phi_f E_f^n - 1 \leq n \leq +1 \quad (25)$$

where n is a function of the morphology of the system.

The most commonly used composite theory model for predicting the stiffness of a composite as a function of aspect ratio was given by Halpin-Tsai. The Halpin-Tsai model is expressed as (Fornes and Paul 2003):

$$\frac{E_c}{E_m} = \frac{1 + \xi \eta \phi_f}{1 - \eta \phi_f} \quad (26)$$

where η is given as (Fornes and Paul 2003):

$$\eta = \frac{\frac{E_f}{E_m} - 1}{\frac{E_f}{E_m} + \xi} \quad (27)$$

ξ is a shape parameter and it depends on the shape and aspect ratio of the filler. ξ is given as (Fornes and Paul 2003):

$$\begin{aligned} \xi &= 2 \left(\frac{L}{t} \right) \quad \text{for longitudinal modulus} \\ \xi &= 2 \quad \text{for transverse modulus} \end{aligned} \quad (28)$$

When the value of ξ becomes very small ($\xi \rightarrow 0$), the Halpin-Tsai model reduces to the inverse of the rule of mixtures (series model):

$$\frac{1}{E_c} = \frac{\phi_f}{E_f} + \frac{1 - \phi_f}{E_m} \quad (29)$$

When the value of ξ becomes very large ($\xi \rightarrow \infty$), the Halpin-Tsai model reduces to the rule of mixtures (parallel model):

$$E_c = (1 - \phi_f)E_m + \phi_f E_f \quad (30)$$

The series model underestimates (lower bound) the value of modulus, whereas the parallel model overestimates (upper bound) the value of modulus. The Halpin-Tsai model leads to results that lie in between these 2 extreme. The Halpin-Tsai model has been shown to predict the values very well at lower filler concentrations. However, it underestimates the values at higher filler concentrations. Therefore, Lewis and Nielsen modified the Halpin-Tsai model to include the maximum volumetric packaging efficiency of the filler. The Modified Halpin-Tsai model is given as (Tucker and Liang 1999):

$$\frac{E_c}{E_m} = \frac{1 + \xi \eta \phi_f}{1 - \varphi \eta \phi_f} \quad (31)$$

where φ can be estimated as (Tucker and Liang 1999):

$$\begin{aligned} \varphi &= 1 + \left(\frac{1 - \phi_m}{\phi_m^2} \right) \phi_f \\ \varphi &= \frac{1}{\phi_f} \left[1 - \exp\left(\frac{-\phi_f}{1 - \frac{\phi_f}{\phi_m}} \right) \right] \end{aligned} \quad (32)$$

Another composite theory that has received considerable attention is the Mori-Tanaka average stress theory. Tandon and Weng (1984) derived complete analytical solutions for the

elastic moduli of an isotropic matrix filled with aligned spherical inclusions as:

$$\frac{E_l}{E_m} = \frac{A}{A + \phi_f (A_1 + 2 \nu_m A_2)} \quad (33)$$

$$\frac{E_t}{E_m} = \frac{2A}{2A + \phi_f [-2\nu_m A_3 + (1 - \nu_m) A_4 + (1 + \nu_m) A_5 A]} \quad (34)$$

where the subscripts l and t denote longitudinal and transverse elastic moduli, respectively, ν_m is the poisson's ratio of the matrix, A , A_1 , A_2 , A_3 , A_4 , and A_5 are parameters that depend on the properties of the filler and the matrix. Complete details of these parameters can be found in Tandon and Weng (1984).

Nielsen (1966) derived an approximate equation for TS_c of composites for the cases of no adhesion between the components. The equation was given as (Nielsen 1966):

$$TS_c = TS_m (1 - \phi_f^{2/3}) S, \quad S \leq 1 \quad (35)$$

where TS_m is the TS of the matrix and S is the stress concentration factor. Verbeek developed a model to predict TS_c of a composite that was based on the average value of TS of individual components. The model was given as (Verbeek 2003):

$$TS_c = (1 - \phi_f) TS_m + K_3 \tau_f (MPF) \quad (36)$$

where K_3 is a correction factor, τ_f is the shear strength of the filler, MPF is the matrix performance factor and is given as (Verbeek 2003):

$$MPF = \phi_f \left(\frac{\alpha}{u} \right) \left(\frac{1}{\tanh(u)} - \frac{1}{u} \right)$$

$$u = \alpha \left(\frac{G_m \phi_f}{E_f (1 - \phi_f)} \right)^{0.5} \quad (37)$$

Several other studies on the modeling of mechanical properties of nanocomposites have been reported (Luo and Daniel 2003; Wang and Pyrz 2004; Wu and others 2004; Weon and Sue 2005; Yan and others 2006; Rao and Pochan 2007; Yung and others 2006). A few studies on the modeling of mechanical properties of bio-nanocomposites using the models discussed above have also been reported (Ray and others 2003b; Peterson and Oksman 2006; Rao 2007). Ray and others (2003b) predicted the storage modulus of bio-nanocomposite films based on poly(butylenes succinate) and modified MMT using the Halpin-Tsai model. There was a good agreement between the predicted values and the experimental values for most of the bio-nanocomposites. Peterson and Oksman (2006) used Halpin-Tsai equation to calculate the theoretical TM for bio-nanocomposites based on PLA and nanoparticles (layered silicate and microcrystalline cellulose). However, there was not a good agreement between the predicted values and the experimental values for both the nanoparticles. Rao (2007) predicted Young's modulus of bio-nanocomposite films based on gelatin and MMT using the rule of mixtures and Halpin-Tsai model. Predicted values of Young's modulus using the Halpin-Tsai model was in agreement with the experimental data, while the rule of mixtures overestimated the values of Young's modulus.

Modeling of barrier properties

Barrier properties of a packaging material are often described by 3 common coefficients—diffusion coefficient, solubility coefficient, and permeability coefficient. The diffusion coefficient (D) describes the movement of permeant molecules through a polymer and is a kinetic property of the polymer-permeant system. The solubility coefficient (S) describes the dissolution of a permeant in a polymer and is a thermodynamic property of the polymer-permeant system. At low concentrations of sorbate, the solubility coefficient is given by Henry's law of solubility as (Hernandez and others 2000):

$$c = Sp \quad (38)$$

where c is the concentration of the sorbate (mol/m^3) and p is the equilibrium vapor pressure of the permeant. The permeability coefficient (P) combines the effects of diffusion and solubility together by incorporating both kinetic and thermodynamic properties of the polymer-permeant system. The permeability coefficient (P) is related to D and S as (Hernandez and others 2000):

$$P = DS \quad (39)$$

This relation holds true when D is independent of concentration and S follows Henry's law. A polymer with good barrier properties has low values of both diffusion and solubility coefficients. For steady state diffusion across a single sheet of a packaging material, P is given as (Hernandez and others 2000):

$$P = \left(\frac{Q}{At} \right) \frac{\Delta x}{\Delta p} = \frac{F \Delta x}{\Delta p} \quad (40)$$

where Q is the total amount of gas that has passed through the material in moles, A is the cross-sectional area in m^2 , t is time in s , Δx is the thickness of the material in m , Δp is the pressure difference across the polymer in Pa , and F is the transmission rate. A related term to describe barrier properties of a polymer is permeance (R) that is defined as (Hernandez and others 2000):

$$R = \frac{P}{\Delta x} = \frac{F}{\Delta p} \quad (41)$$

The effective value of P in polymers is affected by the chemical composition of the polymer and permeant, morphology of the polymer, temperature, T_g of the polymer, and presence of plasticizers and fillers. Change in P with temperature follows an Arrhenius kinetics and the corresponding equation is given as (Hernandez and others 2000):

$$P = P_0 e^{E_p/RT} \quad (42)$$

where E_p is the activation energy (J/mol), R is the gas constant ($8.314 J/mol \cdot K$), P_0 is a preexponential term, and T is temperature in Kelvin.

Bio-nanocomposite polymer films have better barrier properties as compared to homogeneous films even at low solid loadings. Solubility (S_c) of a gas in a bio-nanocomposite can be expressed as (Picard and others 2007):

$$S_c = (1 - \phi_f) S_m \quad (43)$$

where S_m is the solubility of the gas in the matrix. Nanoparticles create a tortuous pathway for the diffusion of gas out of the bio-nanocomposite matrix. This increases the effective path length for diffusion of the gas, thus reducing the diffusion coefficient (D_c). The reduced D_c of a gas in the composite can be expressed as (Picard and others 2007):

$$D_c = \frac{D_m}{\tau} \quad (44)$$

where D_m is the diffusion coefficient in the matrix and τ is the tortuosity factor. Thus, P_c of a bio-nanocomposite can be expressed as:

$$\frac{P_c}{P_m} = \frac{(1 - \phi_f)}{\tau} \quad (45)$$

where P_m is the permeability of the gas in the matrix.

Tortuosity factor for a membrane containing low solid loadings of spheres is given as (Yang and others 2004):

$$\tau = 1 + \frac{\phi_f}{2} \quad (46)$$

Similarly, for a membrane containing periodically arrayed infinite cylinders oriented perpendicular to the direction of diffusion, τ is given as (Yang and others 2004):

$$\tau = 1 + \phi_f \quad (47)$$

Nielsen (1967) considered 2-dimensional (2D) diffusion through a polymer containing infinitely long plates of rectangular cross-section. The tortuosity factor was given as (Nielsen 1967):

$$\tau = 1 + \frac{\alpha \phi_f}{2} \quad (48)$$

where α is the aspect ratio (L/t) and ϕ_f is the volume fraction of the filler. This model assumed that the platelets were fully exfoliated and dispersed along an orientation perpendicular to direction of diffusion.

Bharadwaj (2001) modified the model of Nielsen to include the effect of platelet orientation on the tortuosity factor. The tortuosity factor was given as:

$$\tau = 1 + \frac{\alpha \phi_f}{2} \left(\frac{2}{3} \right) \left(S + \frac{1}{2} \right) \quad (49)$$

where S is an order parameter, given by:

$$S = \frac{1}{2} (3 \cos^2 \theta - 1), \quad -0.5 \leq S \leq 1 \quad (50)$$

Cussler and others (1988) considered rectangular flakes of uniform size dispersed at regular intervals in a composite and proposed the following equation for the tortuosity factor:

$$\tau = 1 + \frac{\alpha^2 \phi_f^2}{4(1 - \phi_f)} + \frac{\sigma \alpha \phi_f}{2} \quad (51)$$

where

$$\alpha = \frac{L}{t}, \quad \sigma = \frac{s}{t}, \quad \phi_f = \frac{L t}{\left(\frac{L}{2} + s \right) (t + b)} \quad (52)$$

where L is the length of the platelets, t is the thickness of the platelets, s is the spacing between the platelets in the direction perpendicular to diffusion, and b is the spacing between the platelets in the direction of diffusion. The parameters α , σ , and ϕ_f are referred to as the aspect ratio, slit shape, and platelet volume fraction, respectively. Cussler and others (1988) also developed a model for tortuosity factor by assuming that flakes were randomly dispersed. The tortuosity factor was given as:

$$\tau = 1 + \frac{\mu \alpha^2 \phi_f^2}{4(1 - \phi_f)} \quad (53)$$

where μ is a combined geometric factor. The values of μ for randomly dispersed flakes of rectangular and hexagonal cross-sections are 0.5 and 0.075.

Another model for tortuosity factor for a composite containing a random array of impermeable barriers was given by Aris as (Falla and others 1996):

$$\tau = 1 + \frac{\alpha^2 \phi_f^2}{4(1 - \phi_f)} + \frac{\alpha \phi_f}{2\sigma} + \frac{2\alpha \phi_f}{\pi(1 - \phi_f)} \ln \left[\frac{\pi \alpha^2 \phi_f}{4\sigma(1 - \phi_f)} \right] \quad (54)$$

The 2nd term on the right-hand side of this equation accounts for the tortuous path that a diffusing molecule must follow. The 3rd term on the right-hand side accounts for the constriction of slits between platelets, and the 4th term on the right-hand side accounts for the resistance of a diffusing species to pass into and out of the narrow slits.

Falla and others (1996) studied diffusion across membranes containing impermeable flakes using Monte Carlo simulation. They showed the effects of tortuous paths around the flakes, diffusion through slits between the flakes, and reduced transport from entering these slits on the diffusion coefficient. They compared the results with the analytical equation developed by Aris. They found that the increase in tortuosity factor was greater for larger aspect ratio (α) and smaller slit shape (σ).

Most of the above-mentioned models for barrier properties have been developed for dilute or semi-dilute and monodispersed systems. These equations are valid for nanocomposites containing exfoliated structures and become less accurate when different types of structures from exfoliated to intercalated exist together (Picard and others 2007). Lape and others (2004) developed a model to predict the tortuosity factor of a polydispersed system. The tortuosity factor was given as (Lape and others 2004):

$$\tau = \left[1 + \left(\frac{1}{3} \frac{\phi_t}{t \sum_i n_i L_i} \right) \sum_i n_i L_i^2 \right]^2 \quad (55)$$

where ϕ_t is the total volume fraction of fillers and n_i is the number of flakes in the size category i .

Gusev and Lusti (2001) developed a finite element model to determine barrier properties of a nanocomposite in which platelets of

nanoparticles were randomly dispersed. Permeability coefficients were calculated on the basis of a linear-response relation between the overall flux and the applied external chemical potential gradient. Numerical results showed that the reduction in permeability was governed by the product of aspect ratio (α) and the volume fraction (ϕ_f) of the platelets. Tortuosity factor was approximated as:

$$\tau = \exp \left[\left(\frac{\alpha \phi_f}{3.47} \right)^{0.71} \right] \quad (56)$$

The results showed that the platelets with aspect ratios greater than 1000 were much more efficient in improving barrier properties of nanocomposites. Their model can be used to identify the role of various morphological imperfections such as incomplete exfoliation, platelet misorientation, and agglomeration in nanocomposites.

Swannack and others (2005) presented 2D and 3-dimensional (3D) Monte Carlo simulation of a polymer-clay nanocomposite system to compute the diffusion coefficients of gas molecules permeating through a nanocomposite film containing oriented platelets. The Monte Carlo method simulated Brownian motion of a small molecule diffusing through a nanocomposite film. 2D and 3D results at low platelet loadings were compared. There were significant differences between the simulation results in 2D and 3D. The 2D simulation predicted a lower value of effective diffusion coefficient than the 3D simulation in most cases. This result is reasonable because 2D simulation is similar to 3D simulation for one infinite platelet dimension. In 3D geometry, platelets are of finite length in both directions perpendicular to the direction of solute transport, thus allowing for more permeation. This resulted in a higher value of effective diffusion coefficient in 3D simulations.

Picard and others (2007) studied polyamide 6-MMT films for a wide range of clay content ranging from 0% to 18% and determined barrier properties for these nanocomposites. Nanocomposites exhibited superior barrier properties to helium, hydrogen, oxygen, and water vapor as compared to that by polyamide film. Different models of monodispersed systems were used to describe the decrease in the permeability value. The model developed by Lape and others (2004), which is based on random distribution of flakes, was found to be the most appropriate model to describe the barrier properties of nanocomposites. All the monodispersed models overestimated the value of the aspect ratio necessary to fit the experimental curves. The model for a polydispersed system given by Lape and others (2004) was also applied to the nanocomposite systems, but the properties of the nanocomposites were not accurately predicted for high concentrations of MMT. The model developed by Lape and others (2004) was modified to account for the distribution of the platelet thickness and contribution of the surfactant layer to the impermeable phase volume fraction for larger agglomerates. The modified tortuosity factor was given as (Picard and others 2007):

$$\tau = \left[1 + \left(\frac{1}{3} \frac{\phi_t}{\sum_i \left(\frac{n_i L_i}{t_i} \right)} \right) \sum_i n_i \left(\frac{L_i}{t_i} \right)^2 \right]^2 \quad (57)$$

The modified model accurately predicted the measured values of permeability in the range of 0% to 18% MMT content.

Several other studies on the modeling of barrier properties of nanocomposites have been reported (Patel and others 2004; Lu and Mai 2005; Sridhar and others 2006; Xu and others 2006). A few studies on the modeling of barrier properties of bio-nanocomposites using the models discussed above have also been reported (Ray and others 2002a, 2003a, 2003b; Park and others 2004; Hedenqvist and others 2006; Peterson and Oksman 2006). Ray and others (2003a) prepared bio-nanocomposites based on PLA and different types of organically modified MMT. OP of the bio-nanocomposites was predicted using the model given by Nielsen (1967). The predicted values were in agreement with the experimental values with Nielsen model slightly over predicting the OP values. Ray and others (2003b) prepared bio-nanocomposites based on polybutylene succinate (PBS) and organically modified MMT. OP of the bio-nanocomposites was predicted using the model given by Nielsen (1967). The results showed that the OP values of bio-nanocomposites were directly related to the aspect ratio of the dispersed clay nanoparticles. OP values decreased with increasing clay content up to 2.8% (w/w), and there was a sharp decrease in OP value with clay content of 3.6% (w/w). This trend was attributed to the sudden increase of aspect ratio above a clay content of 2.8% (w/w) due to a strong flocculation of dispersed clay nanoparticles.

Park and others (2004) prepared bio-nanocomposites based on cellulose acetate, triethyl citrate (as plasticizer), and organically modified clay. WVP of the bio-nanocomposites was predicted using the model given by Cussler and others (1988). The results showed that the predicted and experimental values of WVP were a better fit with higher aspect ratio ($\alpha = 150$) at lower volume fractions ($\phi_f \leq 0.02$), whereas the predicted and experimental values were a better fit with lower aspect ratio ($\alpha = 100$) at higher volume fractions ($\phi_f \geq 0.05$).

Conclusions

Bio-nanocomposites could potentially provide an alternative to the existing plastic packaging materials derived from petroleum. Some of the reasons for unique properties of materials at nanoscale include dominance of electrostatic and van der Waals forces over gravitational and frictional forces, wave-particle duality of electrons, dominance of Brownian motion, higher A_s to V_s ratio, and confinement effect. This article reviews the experimental and modeling techniques to determine properties of bio-nanocomposites based on starch, proteins, and cellulosic polymers. Selection of proper technique to determine properties of these bio-nanocomposites is very critical in assessing their performance for their application as food packaging materials. Tensile testing is used to measure mechanical properties (TM, tensile strength, %E of break) of bio-nanocomposites. Bio-nanocomposites exhibit improved mechanical properties as compared to the biopolymers. This is attributed to the high rigidity and aspect ratio of nanoparticles. WVP and OP are measured to study the effect of nanoparticles on the barrier properties of bio-nanocomposites. Bio-nanocomposites show improved barrier properties as compared to the biopolymers because the dispersed nanoparticles provide a tortuous path for water and gas molecule to pass through. Dynamic mechanical analysis, DSC, and TGA are used to determine the thermal properties of bio-nanocomposites. The improved thermal properties of bio-nanocomposites are attributed to the thermal insulation behavior of the nanoparticles and changes in the dynamics of molecular motion in bio-nanocomposites. Rheological properties are determined by performing steady shear,

dynamic shear, or extensional measurement. Increased viscosity of bio-nanocomposites at low shear rates is attributed to the flow restriction of biopolymer chains in molten state due to the presence of nanoparticles. Mathematical modeling of mechanical and barrier properties of bio-nanocomposites can help in better understanding of the mechanism for much improved properties of bio-nanocomposites. This understanding of mechanism for improved properties of bio-nanocomposites along with proper technique to measure these properties will result in the development of next generation of biodegradable polymers with improved mechanical, barrier, rheological, and thermal properties.

Acknowledgments

Support for the research study undertaken here, resulting in the publication of paper nr FSR-09-36 of the Journal Series of the Dept. of Food, Bioprocessing, and Nutrition Sciences, NCSU, Raleigh, NC 27695-7624 from USDA-NRICGP Grant nr 2008-01503, titled: Development of cross-linked bio-nanocomposite packaging films with enhanced barrier and mechanical properties, is gratefully acknowledged.

The use of trade names in this publication does not imply endorsement by the North Carolina Agricultural Research Service of the products named nor criticism of similar ones not mentioned.

References

- Ahmed S, Jones FR. 1990. A review of particulate reinforcement theories for polymer composites. *J Mater Sci* 25:4933-42.
- Arora A, Padua GW. 2010. Review: nanocomposites in food packaging. *J Food Sci* 75(1):R43-9.
- ASTM Standards. 2002. D882-02. Standard test method for tensile properties of thin plastic sheeting. Philadelphia, Pa.: ASTM Intl.
- ASTM Standards. 2003. D638-03. Standard test method for tensile properties of thin plastics. Philadelphia, Pa.: ASTM Intl.
- ASTM Standards. 2004. E1640-04. Standard test method for assignment of the glass transition temperature by dynamic mechanical analysis. Philadelphia, Pa.: ASTM Intl.
- ASTM Standards. 2005a. E96-05. Standard test methods for water vapor transmission of materials. Philadelphia, Pa.: ASTM Intl.
- ASTM Standards. 2005b. D3985-05. Standard test method for oxygen gas transmission rate through plastic film and sheeting using a coulometric sensor. Philadelphia, Pa.: ASTM Intl.
- ASTM Standards. 2006. D4065-06. Standard practice for plastics: dynamic mechanical properties: determination and report of procedures. Philadelphia, Pa.: ASTM Intl.
- ASTM Standards. 2007. D648-07. Standard test method for deflection temperature of plastics under flexural load in the edgewise position. Philadelphia, Pa.: ASTM Intl.
- ASTM Standards. 2008a. E1356-08. Standard test method for assignment of the glass transition temperatures by differential scanning calorimetry. Philadelphia, Pa.: ASTM Intl.
- ASTM Standards. 2008b. E3418-08. Standard test method for transition temperatures and enthalpies of fusion and crystallization of polymers by differential scanning calorimetry. Philadelphia, Pa.: ASTM Intl.
- ASTM Standards. 2008c. E1131-08. Standard test method for compositional analysis by thermogravimetry. Philadelphia, Pa.: ASTM Intl.
- Azeredo HMC, Mattoso LHC, Avena-Bustillos RJ, Filho GC, Munford ML, Wood D, McHugh TH. 2010. Nanocellulosic reinforced chitosan composite films as affected by nanofiller loading and plasticizer content. *J Food Sci* 75(1):N1-N7.
- Bhardwaj RK. 2001. Modeling the barrier properties of polymer-layered silicate nanocomposites. *Macromolecules* 34:9189-92.
- Bhattacharya SN, Gupta RK, Kamal MR. 2007. Polymeric nanocomposites: theory and practice. Cincinnati: Hanser Gardner Publications, Inc. 383 p.
- Bordes P, Pollet E, Averous L. 2009. Nano-biocomposites: biodegradable polyester/nanoclay systems. *Prog Polym Sci* 34(2):125-55.
- Chang JH, An YU, Sur GS. 2003. Poly(lactic acid) nanocomposites with various organoclays. I. thermomechanical properties, morphology, and gas permeability. *J Polym Sci B Polym Phys* 41:94-103.
- Chang PR, Yang Y, Huang J, Xia W, Feng L, Wu J. 2009. Effects of layered silicate structure on the mechanical properties and structures of protein-based bionanocomposites. *J Appl Polym Sci* 113:1247-56.
- Chen P, Zhang L. 2006. Interaction and properties of highly exfoliated soy protein/montmorillonite nanocomposites. *Biomacromolecules* 7:1700-6.
- Chiou BS, Yee E, Glenn GM, Orts WJ. 2005. Rheology of starch-clay nanocomposites. *Carbohydr Polym* 59:467-75.
- Chiou BS, Wood D, Yee E, Imam SH, Glenn GM, Orts WJ. 2007. Extruded starch-nanoclay nanocomposites: effects of glycerol and nanoclay concentration. *Polym Eng Sci* 47(11):1898-904.
- Chivrac F, Pollet E, Schmutz M, Averous L. 2008. New approach to elaborate exfoliated starch-based nanobiocomposites. *Biomacromolecules* 9:896-900.
- Chivrac F, Pollet E, Averous L. 2009. Progress in nano-bionanocomposites based on polysaccharides and nanoclays. *Mater Sci Eng R* 67:1-17.
- Crosby AJ, Lee JY. 2007. Polymer nanocomposites: the "nano" effect on mechanical properties. *Polym Rev* 47:217-29.
- Cussler E, Hughes SE, Ward WJ, Aris R. 1988. Barrier membranes. *J Memb Sci* 38(2):161-74.

- Damme HV. 2008. Nanocomposites: the end of compromise. In: Brechignac C, Houdy P, Lahmani M, editors. *Nanomaterials and nanochemistry*. New York: Springer. p 348-80.
- De Moura MR, Avena-Bustillos RJ, McHugh TH, Krochta JM, Mattoso LHC. 2008. Properties of novel hydroxypropyl methyl cellulose films containing chitosan nanoparticles. *J Food Sci* 73(7):N31-N37.
- Dogan N, McHugh TH. 2007. Effects of microcrystalline cellulose on functional properties of hydroxyl propyl methyl cellulose microcomposite films. *J Food Sci* 72(1):E16-E22.
- Eijkel JCT, Van Den Berg A. 2005. Nanofluidics: what is it and what can we expect from it. *Microfluid Nanofluidics* 1:249-67.
- Falla WR, Mulski M, Cussler EL. 1996. Estimating diffusion through flake-filled membranes. *J Memb Sci* 119(1):129-38.
- Fornes TD, Paul DR. 2003. Modeling properties of nylon 6/clay nanocomposites using composite theories. *Polymer* 44(17):4993-5013.
- Gusev AA, Lusti HR. 2001. Rational design of nanocomposites for barrier applications. *Adv Mater* 13(21):1641-3.
- Hedenqvist MS, Backman A, Gallstedt M, Boyd RH, Gedde UW. 2006. Morphology and diffusion properties of whey/montmorillonite nanocomposites. *Compos Sci Technol* 66:2350-9.
- Hernandez RJ, Selke SEM, Culter JD. 2000. *Plastic packaging: properties, processing, applications, and regulations*. Cincinnati: Hanser Gardner Publications, Inc. 425 p.
- Huang X, Netravali AN. 2006. Characterization of nano-clay reinforced phytigel-modified soy protein concentrate resin. *Biomacromolecules* 7:2783-9.
- Hubbe MA, Rojas OJ, Lucia LA, Sain M. 2008. Cellulosic nanocomposites: a review. *Biore-sources* 3(3):929-80.
- Jeong HM, Kim BC, Kim EH. 2005. Structure and properties of EVOH/organoclay nanocomposites. *J Mater Sci* 40:3783-7.
- Jones RAL. 2004. *Soft machines: nanotechnology and life*. Oxford: Oxford Univ. Press. 229 p.
- Krishnamachari P, Zhang J, Lou J, Yan J, Uitenham L. 2009. Biodegradable poly(lactic acid)/clay nanocomposites by melt intercalation: a study of morphological, thermal, and mechanical properties. *Int J Polym Anal Character* 14:336-50.
- Krishnamoorti R, Yurekli K. 2001. Rheology of layered silicate nanocomposites. *Curr Opin Colloid and Interface Sci* 6:464-70.
- Lape NK, Nuxoll EE, Cussler EL. 2004. Polydisperse flakes in barrier films. *J Memb Sci* 236(1-2):29-37.
- Li TD, Gao J, Szoszkiewicz R, Landman U, Riedo E. 2007. Structured and viscous water in subnanometer gaps. *Phys Rev B* 75(11):115415.
- Lu C, Mai YW. 2005. Influence of aspect ratio on barrier properties of polymer-clay nanocomposites. *Phys Rev Lett* 95(8):1-4.
- Luo JJ, Daniel IM. 2003. Characterization and modeling of mechanical behavior of polymer/clay nanocomposites. *Compos Sci Technol* 63:1607-16.
- Menard KP. 1999. *Dynamic mechanical analysis a practical introduction*. Boca Raton, Fla.: CRC Press. 208 p.
- Nielsen LE. 1966. Simple theory of stress-strain properties of filler polymers. *J Appl Polym Sci* 10:97-103.
- Nielsen LE. 1967. Models for permeability of filled polymer systems. *J Macromol Sci Part A* 1:929-42.
- Nielsen LE. 1977. Polymeric composite systems with two continuous phases. *J Appl Polym Sci* 21:1579-84.
- Pandey JK, Kumar AP, Misra M, Mohanty AK, Drzal LT, Singh RP. 2005. Recent advances in biodegradable nanocomposites. *J Nanosci Nanotechnol* 5:497-526.
- Park HM, Misra M, Drzal LT, Mohanty AK. 2004. "Green" nanocomposites from cellulose acetate bioplastic and clay: effect of eco-friendly triethyl citrate plasticizer. *Biomacromolecules* 5:2281-8.
- Patel NP, Aberg CM, Sanchez AM, Capracotta MD, Martin JD, Spontak RJ. 2004. Morphological, mechanical, and gas-transport characteristics of crosslinked poly(propylene glycol): homopolymers, nanocomposites and blends. *Polymer* 2004:5941-50.
- Paul MA, Alexandre M, Degee P, Henric C, Rulmont A, Dubois P. 2003. New nanocomposite materials based on plasticized poly(L-lactide) and organo-modified montmorillonites: thermal and morphological study. *Polymer* 44(2):443-50.
- Picard E, Vermogen A, Gerard JF, Espuche E. 2007. Barrier properties of nylon6-montmorillonite nanocomposite membranes prepared by melt blending: influence of the clay content and dispersion rate consequences on modeling. *J Memb Sci* 292(1-2):133-44.
- Peterson L, Oksman K. 2006. Biopolymer based nanocomposites: comparing layered silicates and microcrystalline cellulose as nanoreinforcement. *Compos Sci Technol* 66:2187-96.
- Rao YQ. 2007. Gelatin-clay nanocomposites of improved properties. *Polymer* 48(18):5369-75.
- Rao YQ, Pochan JM. 2007. Mechanics of polymer-clay nanocomposites. *Macromolecules* 40(2):290-6.
- Ray SS, Yamada K, Okamoto M, Ueda K. 2002a. Poly(lactide)-layered silicate nanocomposite: a novel biodegradable material. *Nano Lett* 2(10):1093-6.
- Ray SS, Maiti P, Okamoto M, Yamada K, Ueda K. 2002b. New poly(lactide)/layered silicate nanocomposites. 1. Preparation, characterization, and properties. *Macromolecules* 35:3104-10.
- Ray SS, Yamada K, Okamoto M, Ueda K. 2003a. New poly(lactide)-layered silicate nanocomposites. 2. Concurrent improvements of materials properties, biodegradability and melt rheology. *Polymer* 44:857-66.
- Ray SS, Okamoto K, Okamoto M. 2003b. Structure-property relationship in biodegradable poly(butylene succinate)/layered silicate nanocomposites. *Macromolecules* 36:2355-67.
- Ray SS, Bousmina M. 2005. Biodegradable polymers and their layered silicate nanocomposites: in greening the 21st century materials world. *Prog Mater Sci* 50:962-1079.
- Rhim JW, Hong SI, Park HM, Ng PKW. 2006. Preparation and characterization of chitosan-based nanocomposite films with antimicrobial activity. *J Agric Food Chem* 54:5814-22.
- Rhim JW, Ng PKW. 2007. Natural biopolymer-based nanocomposite films for packaging applications. *Crit Rev Food Sci Nutr* 47(4):411-33.
- Rhim JW, Hong SK, Ha CS. 2009. Tensile, water vapor barrier and antimicrobial properties of PLA/nanoclay composite films. *LWT - Food Sci Technol* 42:612-7.
- Rindusit S, Jingid S, Damrongsakul S, Tiptipakorn S, Takeichi T. 2008. Biodegradability and property characterization of methyl cellulose: effect of nanocompositing and chemical crosslinking. *Carbohydr Polym* 72:444-55.
- Rodmers E. 2006. Size matters: why nanomaterials are different. *Chem Soc Rev* 35:583-92.
- Rogers B, Pennathur S, Adams J. 2008. *Nanotechnology understanding small systems*. Boca Raton: CRC Press. 398 p.

- Romero RB, Leite CAP, Goncalves MC. 2009. The effect of the solvent on the morphology of cellulose acetate/montmorillonite nanocomposites. *Polymer* 50:161–70.
- Roohani M, Habibi Y, Belgacem NM, Ebrahim G, Karimi AN, Dufresne A. 2008. Cellulose whiskers reinforced polyvinyl alcohol copolymers nanocomposites. *Eur Polym J* 44:2489–98.
- Sasmal A, Sahoo D, Nanda R, Nayak P, Nayak PL, Mishra JK, Chang YW, Yoon JY. 2008. Biodegradable nanocomposites from maleated polycaprolactone/soy protein isolate blend with organoclay: preparation, characterization, and properties. *Polym Compos* 30(6):708–14.
- Shelley JS, Mather PT, DeVries KL. 2001. Reinforcement and environmental degradation of nylon-6/clay nanocomposites. *Polymer* 42:5849–58.
- Sheng N, Boyce MC, Parks DM, Rutledge GC, Abes JI, Cohen RE. 2004. Multiscale micromechanical modeling of polymer/clay nanocomposites and the effective clay particle. *Polymer* 45:487–506.
- Shih YF, Wang TY, Jeng RJ, Wu JY, Teng CC. 2007. Biodegradable nanocomposites based on poly(butylene succinate)/organoclay. *J Polym Environ* 15:151–8.
- Sorrentino A, Gorrasi G, Vittoria V. 2007. Potential perspectives of bio-nanocomposites for food packaging applications. *Trends Food Sci Technol* 18:84–95.
- Sridhar LN, Gupta RK, Bhardwaj M. 2006. Barrier properties of polymer nanocomposites. *Ind Eng Chem Res* 45:8282–9.
- Swannack C, Cox C, Liakos A, Hirt D. 2005. A three-dimensional simulation of barrier properties of nanocomposite films. *J Membr Sci* 263(1–2):47–56.
- Tandon GP, Weng GJ. 1984. Effect of aspect ratio of inclusions on the elastic properties of unidirectional aligned composites. *Polym Compos* 5(4):327–33.
- Tang X, Alavi S, Herald TJ. 2008. Barrier and mechanical properties of starch-clay nanocomposite films. *Cereal Chem* 85(3):433–9.
- Tucker CL, Liang E. 1999. Stiffness predictions for unidirectional short-fiber composites: review and evaluation. *Compos Sci Technol* 59:655–71.
- Tunc S, Angellier H, Cahyana Y, Chalier P, Gontard N, Gastaldi E. 2007. Functional properties of wheatgluten/montmorillonite nanocomposite films processed by casting. *J Membr Sci* 289:159–68.
- Valavala PK, Odegard GM. 2005. Modeling techniques for determination of mechanical properties of nanocomposites. *Rev Adv Mater Sci* 9:34–44.
- Verbeek CJR. 2003. The influence of interfacial adhesion, particle size and size distribution on the predicted mechanical properties of particulate thermoplastic composites. *Mater Lett* 57:1919–24.
- Wang J, Pyrz R. 2004. Prediction of the overall moduli of layered silicate-reinforced nanocomposites-part I: basic theory and formulas. *Compos Sci Technol* 64:925–34.
- Wang SF, Shen L, Zhang WD, Tong YJ. 2005. Preparation and mechanical properties of chitosan/carbon nanotubes composites. *Biomacromolecules* 6:3067–72.
- Wang S, Chen L, Tong Y. 2006. Structure-property relationship in chitosan-based biopolymer/montmorillonite nanocomposites. *J Polym Sci A Polym Chem* 44:686–96.
- Weon JI, Sue HJ. 2005. Effects of clay orientation and aspect ratio on mechanical behavior of nylon-6 nanocomposite. *Polymer* 46:6325–34.
- Wu YP, Jia QX, Yu DS, Zhang LQ. 2004. Modeling young's modulus of rubber-clay nanocomposites using composite theories. *Polym Test* 23:903–9.
- Xu B, Zheng Q, Song Y, Shangguang Y. 2006. Calculating barrier properties of polymer/clay nanocomposites: effects of clay layers. *Polymer* 47:2904–10.
- Yan W, Lin RJT, Bhattacharyya D. 2006. Particulate reinforced rotationally moulded polyethylene composites – mixing methods and mechanical properties. *Compos Sci Technol* 66:2080–8.
- Yang C, Smyrl WH, Cussler EL. 2004. Flake alignment in composite coatings. *J Membr Sci* 231:1–12.
- Yang KK, Wang XL, Wang YZ. 2007. Progress in nanocomposite of biodegradable polymer. *J Ind Eng Chem* 13(4):485–500.
- Yu J, Cui G, Wei M, Huan J. 2007. Facile exfoliation of rectorite nanoplatelets in soy protein matrix and reinforced bio-nanocomposites thereof. *J Appl Polym Sci* 104:3367–77.
- Yung KC, Wang J, Yue TM. 2006. Modeling Young's modulus of a polymer-layered silicate nanocomposites using a modified Halpin-Tsai micromechanical model. *J Reinforced Plastics Compos* 25(8):847–61.
- Zhao R, Torley P, Halley PJ. 2008. Emerging biodegradable materials: starch- and protein-based bio-nanocomposites. *J Mater Sci* 43:3058–71.
- Zheng H, Ai F, Wei M, Huang J, Chang PR. 2007. Thermoplastic soy protein nanocomposites reinforced by carbon nanotubes. *Macromol Mater Eng* 292:780–8.